Computers & Geosciences 43 (2012) 83–89

Contents lists available at SciVerse ScienceDirect

Computers & Geosciences

journal homepage: www.elsevier.com/locate/cageo

Oscillatory numerical experiments in finely layered anisotropic viscoelastic media

Stefano Picotti [a,*], José M. Carcione [a], Juan E. Santos [b,c,d]

[a] Istituto Nazionale di Oceanografia e di Geofisica Sperimentale (OGS), Borgo Grotta Gigante 42c, 34010 Sgonico, Trieste, Italy
[b] CONICET, Instituto del Gas y del Petróleo, Facultad de Ingeníeria, Universidad de Buenos Aires, Av. Las Heras 2214 Piso 3 C1127AAR Buenos Aires, Argentina
[c] Universidad Nacional de La Plata, La Plata, Argentina
[d] Department of Mathematics, Purdue University, 150 N. University Street, West Lafayette, IN 47907-2067, USA

ARTICLE INFO

Article history:
Received 11 August 2011
Received in revised form
11 December 2011
Accepted 26 February 2012
Available online 3 March 2012

Keywords:
Backus averaging
Viscoelasticity
Anisotropy
FE method

ABSTRACT

A finely layered medium behaves as a homogeneous anisotropic medium at long wavelengths. When each layer is a transversely isotropic viscoelastic (TIV) medium, attenuation anisotropy can be described by a generalization of Backus averaging to the lossy case. We introduce a method to compute the complex and frequency-dependent stiffnesses of the equivalent viscoelastic, homogeneous, transversely isotropic medium from numerical simulations of oscillatory (harmonic) tests based on a space–frequency domain finite-element (FE) method. We apply the methodology to a periodic sequence of shale and limestone thin layers and determine the energy velocities and quality factors of the qP-, qSV- and SH-wave modes as a function of frequency and propagation direction. The agreement between theory and numerical experiments is very good when the long-wavelength condition is satisfied.

1. Introduction

Many geological systems, as for instance fluvial and lacustrine depositional formations, are composed of very thin layers with varying viscoelastic properties and cannot be correctly described by isotropic rheological equations, requiring to be modeled as transversely isotropic media. This occurs when the dominant wavelength of the seismic signal is much larger than the thickness of the single layers. The medium is seen by the signal as transversely isotropic with a vertical axis of symmetry (Backus, 1962; Carcione, 2007).

Each single layer is transversely isotropic in many situations. For instance, the elastic properties of shales are strongly affected by the presence of clay minerals, controlling in particular the degree of anisotropy. In fact, monocrystals of clay minerals are very thin platelets whose aggregates may exhibit considerable anisotropy of elastic properties (Bayuk et al., 2007). During deposition at the sediment–water interface, clays have a high porosity because sedimentation occurs more commonly as flocculated clay aggregates having random orientation of clay particles. With increasing overburden pressures, mechanical compaction and dewatering processes reduces the porosity because the platy clay domains tend to collapse generating a preferred orientation (Revil et al., 2002), which is generally perpendicular to the direction of maximum compaction stress. Bottom currents can also reorient the grains to a more preferred orientation. Other examples of intrinsic anisotropic materials are biogenic carbonates. Having studied many sediment samples from core drilling sites, Carlson and Christensen (1979) suggested that in chalks and limestones the phenomenon results from the preferred orientation of calcite grains, rather than the alignment of cracks and pores in the sediment. Carlson et al. (1984) concluded that carbonate-bearing deep-sea sediments may be regarded as transversely isotropic media with symmetry axes normal to bedding. Moreover, the system studied in this work can be of interest in the theory of composites, where fibers in the form of sheets or material variations are usually used to deliberately make the composite anisotropic along a given direction to induce maximum stiffness (Amirkhizi et al., 2010).

To our knowledge, the first researcher to study the anisotropic character of finely layered media was Bruggeman (1937). Others analyzed the problem using alternative approaches, e.g., Riznichenko (1949) and Postma (1955), who considered a two-constituent periodically layered medium. Later, Backus (1962) showed that a system composed of several thin layers is equivalent (each layer is assumed thin relative to the dominant wavelength) to a homogeneous, transversely isotropic medium, and that the properties of this equivalent medium can be derived using appropriate averaging techniques. Backus also obtained the average elasticity constants in the more general case when the single layers are transversely isotropic with the symmetry axis perpendicular to the layering plane. Moreover, he assumed

* Corresponding author. Tel.: +39 040 2140280; fax: +39 40 327521.
E-mail addresses: spicotti@inogs.it (S. Picotti), jcarcione@inogs.it (J.M. Carcione), santos@fcaglp.fcaglp.unlp.edu.ar (J.E. Santos).

0098-3004/$ - see front matter © 2012 Elsevier Ltd. All rights reserved.
doi:10.1016/j.cageo.2012.02.026

stationarity, i.e., in a given length of composite medium much smaller than the wavelength, the proportion of each material is constant (periodicity is not required).

Schoenberg and Muir (1989) extended Backus approach to single layers of arbitrary anisotropic layers using a matrix formalism. However, this generalization has been questioned by Hudson and Crampin (1991), who state that the theory cannot be applied to oblique sets of layers or cracks (even for weak anisotropy), since the structure is no longer one-dimensional and Backus's assumptions are invalidated. In this paper, we consider single transversely isotropic viscoelastic (TIV) layers with a vertical symmetry axis. The test of Schoenberg and Muir's theory in the lossless and anelastic cases is a topic of future research.

Backus averaging for the lossless case has been verified numerically by Carcione et al. (1991), who found that the minimum ratio between the P-wave dominant pulse wavelength and the spatial period of the layering depends on the contrast between the constituents. For instance, for a periodic sequence of epoxy-glass it is approximately 8, and for sandstone-limestone (which has a lower reflection coefficient) it is between 5 and 6. In any case, an optimal ratio can be found for which the equivalence between a finely layered medium and a homogeneous transversely isotropic medium is valid. Carcione (1992) generalized Backus averaging to the anelastic case, obtaining the first model for Q-anisotropy (see Carcione, 2007), hereafter referred to as the Backus–Carcione theory. Other alternative models of Q-anisotropy were proposed by Carcione and Cavallini (1994, 1995) and Carcione et al. (1998). A brief description of all these models can be found in Carcione (2007).

Picotti et al. (2010) and Santos et al. (2011) were the first to test Backus–Carcione theory, introducing a novel method to obtain the complex and frequency-dependent stiffnesses from numerical simulations of oscillatory (harmonic) tests. They applied the methodology to a shale-limestone and epoxy-glass periodic sequence of thin layers, and computed the quality factor and wave velocities as a function of frequency and propagation direction. This analysis indicates that attenuation anisotropy due to fine-layering is more pronounced for shear waves than for compressional waves. Moreover, attenuation is higher in the direction perpendicular to layering or close to it. Using a similar approach, Picotti et al. (2010) and Santos et al. (2011) considered isotropic layers, while Carcione et al. (2011) and Krzikalla and Müller (2010) extended the methodology to poroelastic media, obtaining the five complex and frequency-dependent stiffnesses of the equivalent viscoelastic medium.

In order to test the general Backus–Carcione theory for Q-anisotropy, we perform numerical simulations using an upscaling procedure to obtain the complex stiffnesses of the effective viscoelastic transversely isotropic medium. This is the generalized version to the TIV case of the procedure used by Picotti et al. (2010) and Santos et al. (2011). It consists of the simulation of oscillatory compressibility and shear tests based on a space–frequency domain FE method. First, we use the FE method at a single frequency to approximate the solutions of the associated boundary value problems and obtain the effective complex stiffnesses versus frequency. Then, quality factors and energy velocities as a function of frequency and propagation angle are computed, using the complex stiffnesses obtained numerically and analytically. Finally, we compare the two results and validate the theory, discussing the differences with the results using isotropic layers (Picotti et al., 2010).

2. Generalized viscoelastic Backus averaging

We consider that each thin layer is a TIV medium that can be described by the model developed by Carcione (1990). The complex stiffnesses, in Voigt's notation, are given by (Carcione, 2007)

$$p_{I(I)} = c_{I(I)} - \overline{\mathcal{E}} + \overline{\mathcal{K}} M_1 + \tfrac{4}{3}\overline{\mu} M_2, \tag{2.1}$$

$$p_{IJ} = c_{IJ} - \overline{\mathcal{E}} + \overline{\mathcal{K}} M_1 + 2\overline{\mu}(1 - \tfrac{1}{3}M_2), \quad I,J = 1,2,3; \ I \neq J, \tag{2.2}$$

$$p_{44} = p_{55} = c_{55} M_2, \quad p_{66} = c_{66} + \overline{\mu}(M_2 - 1), \tag{2.3}$$

where

$$\overline{\mathcal{K}} = \overline{\mathcal{E}} - \tfrac{4}{3}\overline{\mu} \tag{2.4}$$

and

$$\overline{\mathcal{E}} = \frac{1}{3}\sum_{I=1}^{3} c_{II}, \quad \overline{\mu} = \frac{1}{3}\sum_{I=4}^{6} c_{II}. \tag{2.5}$$

Here, M_1 and M_2 are frequency-dependent complex functions corresponding to dilatational and shear deformations, respectively, and c_{IJ} are the unrelaxed (high-frequency limit) stiffness components.

To quantify the anisotropy of each thin layer, we use Thomsen's (1986) coefficients:

$$\epsilon = \frac{c_{11} - c_{33}}{2c_{33}},$$

$$\gamma = \frac{c_{66} - c_{55}}{2c_{55}},$$

$$\delta = \frac{(c_{13} + c_{55})^2 - (c_{33} - c_{55})^2}{2c_{33}(c_{33} - c_{55})}. \tag{2.6}$$

If c_P and c_S are the elastic high-frequency limit compressional- and shear-wave velocities, and ρ is the density, the coefficients c_{33} and c_{55} are given by

$$c_{33} = \rho c_P^2, \quad c_{55} = \rho c_S^2. \tag{2.7}$$

The other three coefficients, c_{11}, c_{66} and c_{13}, can be obtained from Eq. (2.6). According to Carcione (1992), the equivalent TIV is defined by the following complex stiffnesses:

$$\overline{p}_{11} = \langle p_{11} - p_{13}^2 p_{33}^{-1} \rangle + \langle p_{33}^{-1} \rangle^{-1} \langle p_{33}^{-1} p_{13} \rangle^2,$$

$$\overline{p}_{33} = \langle p_{33}^{-1} \rangle^{-1},$$

$$\overline{p}_{13} = \langle p_{33}^{-1} \rangle^{-1} \langle p_{33}^{-1} p_{13} \rangle,$$

$$\overline{p}_{55} = \langle p_{55}^{-1} \rangle^{-1},$$

$$\overline{p}_{66} = \langle p_{66} \rangle, \tag{2.8}$$

where the thickness weighted average of a quantity a is defined as

$$\langle a \rangle = \sum_{l=1}^{L} q_l a_l, \tag{2.9}$$

where q_l is the relative thickness of material l. In the case of a periodic sequence of two alternating layers, Eq. (2.8) are similar to those of Postma (1955), who considered lossless layers.

The method is valid for any complex modulus describing the anelastic properties of the medium. Here, we assume constant quality factors over the frequency range of interest (until about 100 Hz). Such behavior is modeled by a continuous distribution of relaxation mechanisms based on the standard linear solid (Liu et al., 1976, Ben-Menahem and Singh, 1981, p. 909; Carcione, 2007). The dimensionless dilatational and shear complex moduli for a specific frequency can be expressed as

$$M_v(\omega) = \left(1 + \frac{2}{\pi Q_{0v}} \ln \frac{1 + i\omega\tau_2}{1 + i\omega\tau_1}\right)^{-1}, \quad v = 1,2, \tag{2.10}$$

where ω is the angular frequency, $i=\sqrt{-1}$, τ_1 and τ_2 are time constants, with $\tau_2<\tau_1$, and Q_{0v} defines the value of the quality factor which remains nearly constant over the selected frequency range.

An alternative model describing the relaxation mechanism is a single Zener element. The complex moduli associated with bulk and shear deformations of a Zener element can be expressed as

$$M_v=\frac{1+i\omega\tau_\epsilon^{(v)}}{1+i\omega\tau_\sigma^{(v)}},\quad v=1,2, \tag{2.11}$$

where $\tau_\sigma^{(v)}$ and $\tau_\epsilon^{(v)}$ are relaxation times. They are given by

$$\tau_\epsilon^{(v)}=\frac{\tau_0}{Q_{0v}}(\sqrt{Q_{0v}^2+1}+1),\quad \tau_\sigma^{(v)}=\tau_\epsilon^{(v)}-\frac{2\tau_0}{Q_{0v}}, \tag{2.12}$$

where τ_0 is a relaxation time such that $1/\tau_0$ is the center frequency of the relaxation peak and Q_{0v} are the minimum dilatational and shear quality factors.

3. Determination of the stiffnesses

In order to determine the coefficients in Eqs. (B.9)–(B.14) we proceed as follows (see also Picotti et al., 2010; Santos et al., 2011; Carcione et al., 2011.) We solve Eq. (B.8) in the 2D case on a reference square $\Omega=(0,L)^2$ with boundary Γ in the (x_1,x_3)-plane. Set $\Gamma=\Gamma^L\cup\Gamma^B\cup\Gamma^R\cup\Gamma^T$, where

$$\Gamma^L=\{(x_1,x_3)\in\Gamma: x_1=0\},\quad \Gamma^R=\{(x_1,x_3)\in\Gamma: x_1=L\},$$

$$\Gamma^B=\{(x_1,x_3)\in\Gamma: x_3=0\},\quad \Gamma^T=\{(x_1,x_3)\in\Gamma: x_3=L\}.$$

Denote by ν the unit outer normal on Γ and let χ be a unit tangent on Γ so that $\{\nu,\chi\}$ is an orthonormal system on Γ. The sample is subjected to time-harmonic compressions $\Delta Pe^{i\omega t}$, where P denotes pressure, and time-harmonic tangential forces $\Delta Ge^{i\omega t}$, where G is the shear stress (see Fig. 1). Moreover, denote by u and σ the displacement and stress vectors.

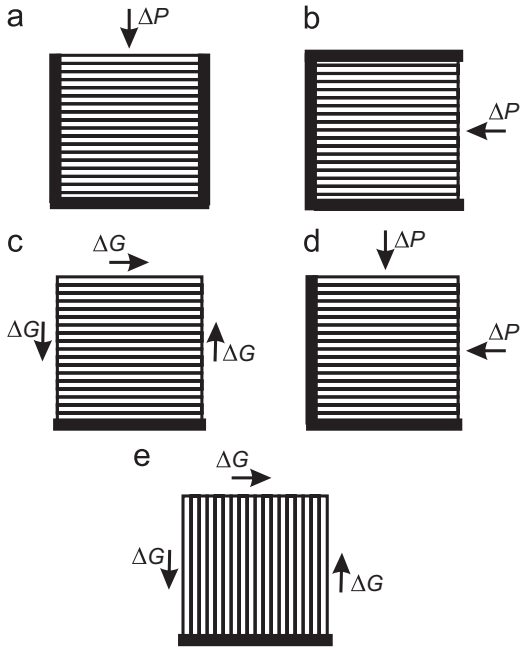

Fig. 1. Oscillatory tests performed to obtain $\overline{p}_{33}$ (a), $\overline{p}_{11}$ (b), $\overline{p}_{55}$ (c), $\overline{p}_{13}$ (d) and $\overline{p}_{66}$ (e). The orientation of the layers and the directions of the applied stresses are indicated. The thick black lines at the edges indicate rigid boundary conditions, as described by equations (3.3), (3.7), (3.9) and (3.13).

It follows how to obtain the stiffness components.

(i) $\overline{p}_{33}$: We solve Eq. (B.8) in Ω with the following boundary conditions:

$$\sigma(u)\nu\cdot\nu=-\Delta P,\quad (x_1,x_3)\in\Gamma^T, \tag{3.1}$$

$$\sigma(u)\nu\cdot\chi=0,\quad (x_1,x_3)\in\Gamma, \tag{3.2}$$

$$u\cdot\nu=0,\quad (x_1,x_3)\in\Gamma^L\cup\Gamma^R\cup\Gamma^B. \tag{3.3}$$

In this experiment $\epsilon_{11}(u)=\epsilon_{22}(u)=0$ and from Eq. (B.11) we see that this experiment determines $\overline{p}_{33}$ as follows.

Denoting by V the original volume of the sample and by $\Delta V(\omega)$ its (complex) oscillatory volume change, we note that

$$\frac{\Delta V(\omega)}{V}=-\frac{\Delta P}{\overline{p}_{33}(\omega)}, \tag{3.4}$$

valid in the quasi-static case. After solving Eq. (B.8) with the boundary conditions (3.1)–(3.3), the vertical displacements $u_3(x,L,\omega)$ on Γ^T allow us to obtain an average vertical displacement $u_3^T(\omega)$ at the boundary Γ^T. Then, for each frequency ω, the volume change produced by the compressibility test can be approximated by $\Delta V(\omega)\approx Lu_3^T(\omega)$, which enable us to compute $\overline{p}_{33}(\omega)$ by using the relation (3.4).

(ii) $\overline{p}_{11}$: The boundary conditions are

$$\sigma(u)\nu\cdot\nu=-\Delta P,\quad (x_1,x_3)\in\Gamma^R, \tag{3.5}$$

$$\sigma(u)\nu\cdot\chi=0,\quad (x_1,x_3)\in\Gamma, \tag{3.6}$$

$$u\cdot\nu=0,\quad (x_1,x_3)\in\Gamma^L\cup\Gamma^B\cup\Gamma^T. \tag{3.7}$$

In this experiment, $\epsilon_{33}(u)=\epsilon_{22}(u)=0$ and from Eq. (B.9) we have that this experiment determines $\overline{p}_{11}$ in the same way indicated for $\overline{p}_{33}$.

(iii) $\overline{p}_{55}$: The boundary conditions are

$$\sigma(u)\chi=g,\quad (x_1,x_3)\in\Gamma^T\cup\Gamma^L\cup\Gamma^R, \tag{3.8}$$

$$u=0,\quad (x_1,x_3)\in\Gamma^B, \tag{3.9}$$

where

$$g=\begin{cases}(0,-\Delta G), & (x_1,x_3)\in\Gamma^L,\\ (0,\Delta G), & (x_1,x_3)\in\Gamma^R,\\ (\Delta G,0), & (x_1,x_3)\in\Gamma^T.\end{cases}$$

The change in shape of the rock sample allow us to compute $\overline{p}_{55}(\omega)$ by using the relation

$$\tan[\theta(\omega)]=\frac{\Delta G}{\overline{p}_{55}(\omega)}, \tag{3.10}$$

where $\theta(\omega)$ is the angle between the original positions of the lateral boundaries and the location after applying the shear stresses (Kolsky, 1963).

The horizontal displacements $u_1(x_1,L,\omega)$ at the top boundary Γ^T are used to obtain, for each frequency, an average horizontal displacement $u_1^T(\omega)$ at the boundary Γ^T. This average value allows us to approximate the change in shape suffered by the sample, given by $\tan[\theta(\omega)]\approx u_1^T(\omega)/L$, which from Eq. (3.10) yields $\overline{p}_{55}(\omega)$.

(iv) $\overline{p}_{66}$: Since this stiffness is associated with shear waves traveling in the (x_1,x_2)-plane, we take the layered sample, rotate it 90° and apply the shear test as indicated for $\overline{p}_{55}$.

(v) $\overline{p}_{13}$: The boundary conditions

$$\sigma(u)\nu\cdot\nu=-\Delta P,\quad (x_1,x_3)\in\Gamma^R\cup\Gamma^T, \tag{3.11}$$

$$\sigma(u)\nu\cdot\chi=0,\quad (x_1,x_3)\in\Gamma, \tag{3.12}$$

$$u\cdot\nu=0,\quad (x_1,x_3)\in\Gamma^L\cup\Gamma^B. \tag{3.13}$$

Thus, in this experiment $\epsilon_{22}=0$, and from Eqs. (B.9) and (B.11) we get

$$\tau_{11}=\overline{p}_{11}\epsilon_{11}+\overline{p}_{13}\epsilon_{33},$$

$$\tau_{33}=\overline{p}_{13}\epsilon_{11}+\overline{p}_{33}\epsilon_{33}, \tag{3.14}$$

where ϵ_{11} and ϵ_{33} are the strain components at the right lateral side and top side of the sample, respectively. Then from Eq. (3.14) and using $\tau_{11}=\tau_{33}=-\Delta P$ [cf. Eq. (3.11)], we obtain $\overline{p}_{13}(\omega)$ as

$$\overline{p}_{13}(\omega)=\frac{\overline{p}_{11}\epsilon_{11}-\overline{p}_{33}\epsilon_{33}}{\epsilon_{11}-\epsilon_{33}}. \tag{3.15}$$

To estimate the effective complex stiffnesses, we use a FE procedure to approximate the solution of the equations of motion (B.8) under the boundary conditions described above. We use bilinear functions to approximate the solid displacement vector. The variational formulation for the boundary-value problems defined in this section, as well as the FE method is analogous to that stated in Santos et al. (2011). The results on the existence and uniqueness of the solution of the continuous and discrete problems presented in that reference can be extended to the TIV case here analyzed. Also, a generalization of the argument given in Santos et al. (2011) would yield a priori error estimates of order $h^{3/2}$ in the L^2-norm and $h^{1/2}$ in the H^1-energy norm, h being the size of the computational mesh.

Table 1
Material properties.

Medium	ρ (kg/m^3)	c_P (m/s)	c_S (m/s)	Q_{01}	Q_{02}	ϵ	γ	δ
Shale	2250	2074	869	60	20	0.110	0.165	0.090
Limestone	2700	5443	3043	80	40	0.056	0.067	−0.003

4. Example

The example considers the shale-limestone periodic layered medium described in Carcione (1992), where each layer is a TIV medium. The properties are given in Table 1, where the anisotropic coefficients are taken from Thomsen (1986) and Wang (2002). Let the time constants in Eq. (2.10) be $\tau_1=0.16$ s and $\tau_2=0.3$ ms, so that the quality factor of each single isotropic layer is nearly constant over the exploration seismic band (from about 10 Hz to 100 Hz). In the long-wavelength limit, the medium is

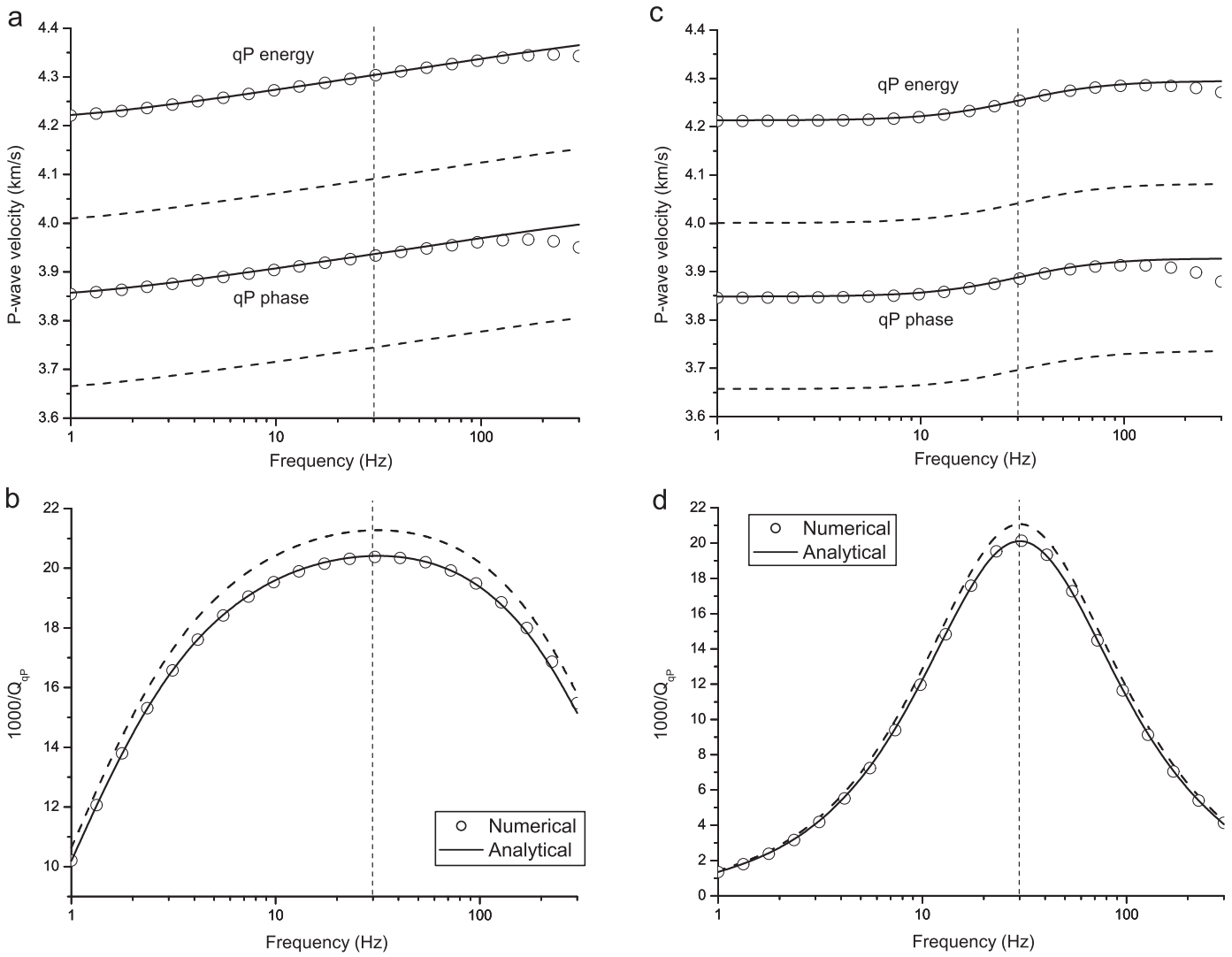

Fig. 2. qP-wave phase and energy velocities (a) and quality factor (b) as a function of frequency obtained with the oscillatory tests (symbols) and Backus–Carcione theory (solid line). The propagation angle is $\theta=60^\circ$. We observe an excellent agreement until about 300 Hz. The dashed curves represent the results obtained by Picotti et al. (2010) using isotropic layers, while (c) and (d) show the same curves obtained using a single Zener element with a relaxation frequency of 30 Hz to describe the anelastic properties of the medium.

described by the Backus averaging relations (2.8), the phase velocities (A.2), the energy velocities (A.3) and (A.7), and the quality factors (A.10). In order to validate the Backus theory we perform the numerical compressibility and shear oscillatory tests described in the previous section. The stratified medium is a 50 cm side sample composed by 100 alternating plane layers of shale and limestone of equal thickness. The spatial period of the layering is then 1 cm. The simulations use a uniform mesh of 100×100 elements.

Fig. 2 shows the qP-wave phase and energy velocities (a) and quality factor (b) as a function of frequency obtained with the oscillatory tests (symbols), compared to Backus theory, generalized to the lossy case by Carcione (1992) (solid line). The dashed curves represent the results obtained by Picotti et al. (2010) using isotropic layers, while (c) and (d) show the same curves obtained using a single Zener element [cf. Eq. (2.11)] with a relaxation frequency of 30 Hz to describe the anelastic properties of the medium. These figures show how the model for the relaxation mechanism influences the velocity and attenuation plots versus frequency.

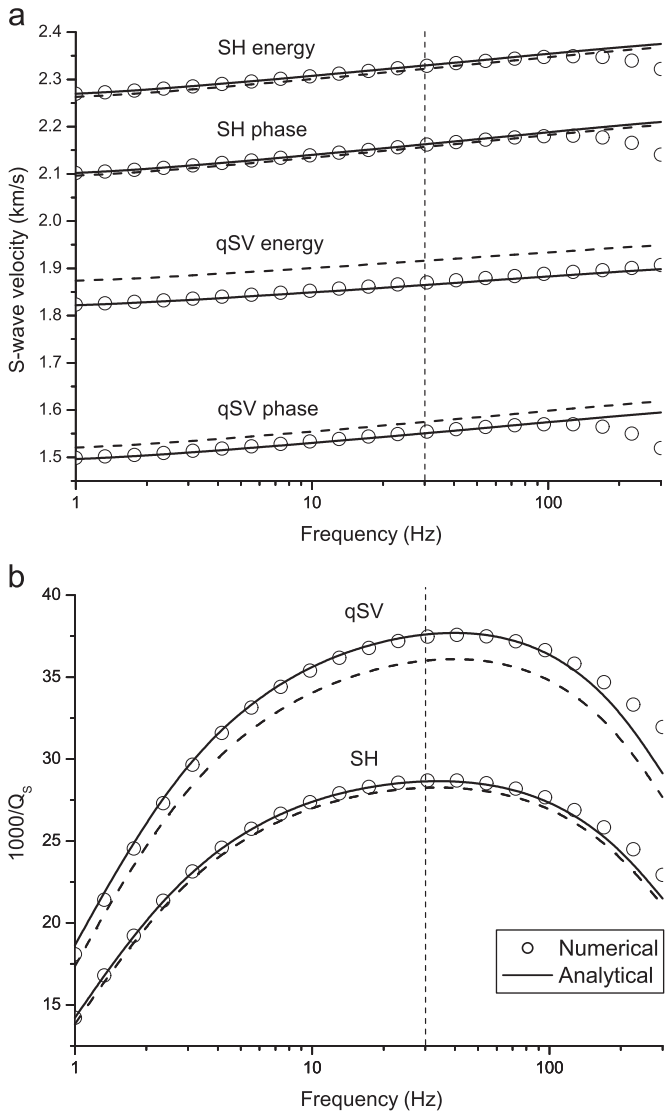

Fig. 3. S-wave phase and energy velocities (a) and quality factor (b) as a function of frequency obtained with the oscillatory tests (symbols) and Backus–Carcione theory (solid line). The propagation angle is $\theta = 60^\circ$. We observe an excellent agreement until about 300 Hz. The dashed curves represent the results obtained by Picotti et al. (2010) using isotropic layers.

Fig. 3 displays the same results obtained for the shear waves. The propagation angle corresponding to the phase velocity is $\theta = 60^\circ$ (dashed line). The corresponding energy angles are $\psi = 83.8^\circ$ for the qP wave, $\psi = 26.3^\circ$ for the qSV wave and

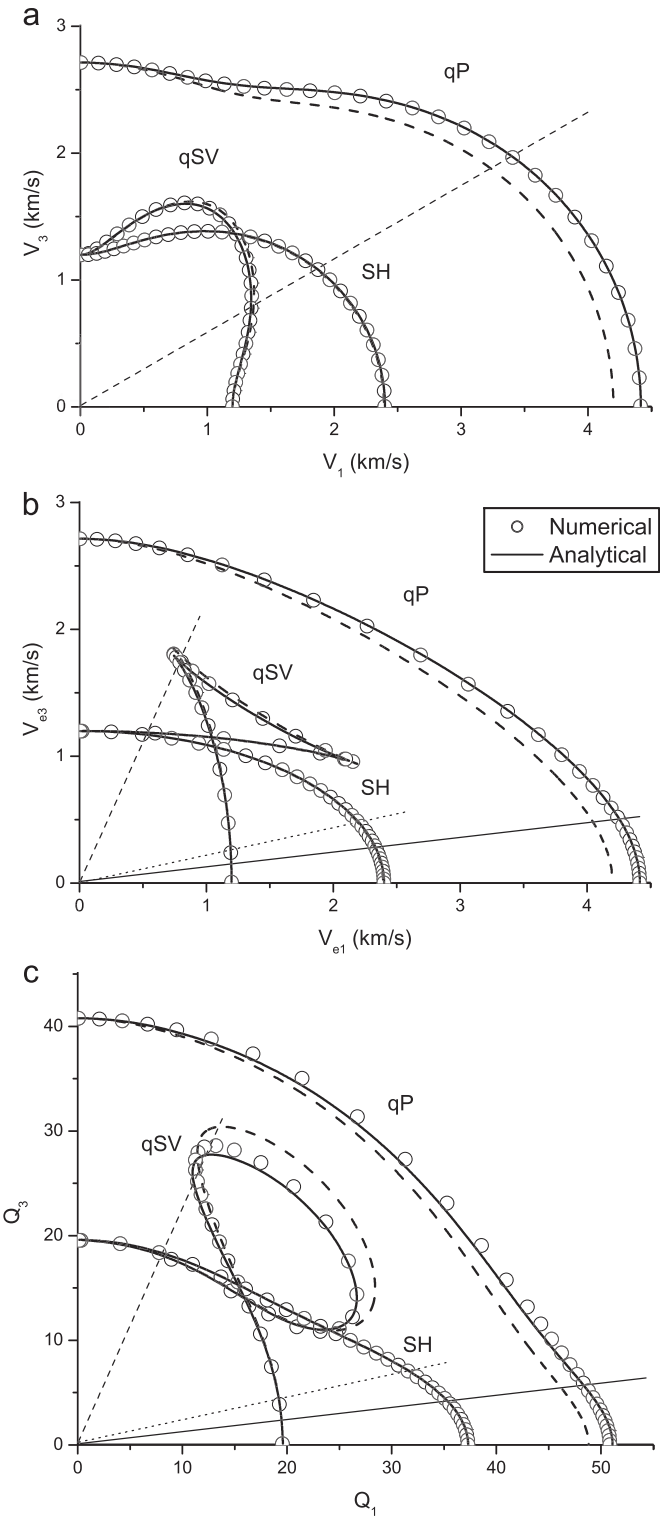

Fig. 4. Polar representation of the phase velocity (a), energy velocity (b) and quality factor (c) corresponding to a frequency of 30 Hz (the vertical dashed lines indicated in Figs. 2 and 3). The symbols represent the numerical simulations. The dashed line in (a) corresponds to the phase angle $\theta = 60^\circ$. The solid, dashed and dotted lines in (b) and (c) correspond to the energy angles $\psi = 83.8^\circ$ (qP wave), $\psi = 26.3^\circ$ (qSV wave) and $\psi = 81.8^\circ$ (SH wave). The dashed curves represent the results obtained by Picotti et al. (2010) using isotropic layers.

$\psi = 81.8^\circ$ for the SH wave. It is seen that anisotropy implies quite different phase and energy velocity curves. We observe an excellent agreement between the theoretical and numerical results until about 300 Hz.

Fig. 4 shows polar representations of the phase velocity (a), energy velocity (b) and quality factor (c) at 30 Hz. The polar curve for the quality factor is given by $(\sin\psi, \cos\psi)Q$. Both the phase and energy angles are indicated. As before, the agreement is excellent. This plot shows that attenuation anisotropy due to fine-layering is more pronounced for shear waves than for compressional waves. Moreover, the intrinsic layer anisotropy affects more the quality factors than the velocities, in particular for qSV and qP waves (compare to the isotropic case). In this case, the qP-, qSV- and SH-wave wavelengths along the symmetry axis ($\theta = 0$) are 92 and 42 m, respectively. Therefore the dominant wavelength (at 30 Hz) to spatial period ratio is 9200 and 4200, respectively, i.e., well within the long-wavelength limit (which, in theory, is between 5 and 8 for P waves approximately, and depending on the single constituents).

5. Conclusions

The general Backus–Carcione theory describes the stiffnesses and the anisotropic attenuation features of finely layered media at long wavelengths, when each layer is a transversely isotropic viscoelastic medium. The effective medium has the same material symmetry. These systems can be found in many geological environments, as for instance fluvial, lacustrine, and deep marine sediments, where shales and carbonates are generally found to be intrinsically anisotropic, and in man-made composites, designed for specific purposes.

To test the theory, we have adapted a numerical method based on oscillatory experiments introduced by the same authors in previous works, i.e., we obtain the complex and frequency-dependent stiffnesses which allow us to compute the wave velocities and quality factors as a function of frequency and propagation angle. The methodology is based on a finite-element solution of the equations of motion in the space–frequency domain to simulate harmonic compressibility and shear tests. We consider a periodic sequence of shale and limestone anisotropic layers. The agreement between the numerical and theoretical results is excellent. The method validates the anelastic theory for Q-anisotropy and, in addition, the expressions of the wave velocities and Q factors for homogeneous viscoelastic body waves in anisotropic media. Moreover, the results of the experiments show that layering anisotropy is more pronounced for shear waves than for compressional waves, while intrinsic layer anisotropy affects more the quality factors than the velocities, in particular for qSV and qP waves.

Since attenuation anisotropy is more pronounced than velocity anisotropy, Q-anisotropy estimation may provide more reliable information about the orientation of layering and fractures. Shear-wave experiments can provide useful information, since it is seen that attenuation anisotropy due to fine-layering and intrinsic anisotropy is more pronounced for shear waves than for compressional waves. In poroelasticity, attenuation anisotropy provides additional information for hydrocarbon reservoirs characterization, because it may be used as an indicator of permeability and fluid saturation.

The theory and numerical solver proposed in this work can be applied to more complex geological systems and man-made composite (lower symmetries, stochastic heterogeneities, fractures, cracks, etc.).

Appendix A. Propagation properties

We consider homogeneous viscoelastic waves for which the propagation and attenuation directions coincide (e.g., Carcione, 2007). The complex velocities are the key quantity to obtain the wave velocities and quality factor of the equivalent anisotropic medium. They are given by

$$v_{\rm qP} = (2\overline{\rho})^{-1/2}\sqrt{\overline{p}_{11}l_1^2 + \overline{p}_{33}l_3^2 + \overline{p}_{55} + A},$$

$$v_{\rm qSV} = (2\overline{\rho})^{-1/2}\sqrt{\overline{p}_{11}l_1^2 + \overline{p}_{33}l_3^2 + \overline{p}_{55} - A},$$

$$v_{\rm SH} = \overline{\rho}^{-1/2}\sqrt{\overline{p}_{66}l_1^2 + \overline{p}_{55}l_3^2}$$

$$A = \sqrt{[(\overline{p}_{11} - \overline{p}_{55})l_1^2 + (\overline{p}_{55} - \overline{p}_{33})l_3^2]^2 + 4[(\overline{p}_{13} + \overline{p}_{55})l_1 l_3]^2}. \tag{A.1}$$

(Auld, 1990; Carcione, 2007, Eq. (1.79)), where $\overline{\rho} = \langle \rho \rangle$, $l_1 = \sin\theta$ and $l_3 = \cos\theta$ are the directions cosines, θ is the propagation angle between the wavenumber vector and the symmetry axis, and the three velocities correspond to the qP, qSV and SH waves, respectively. The phase velocity is given by

$$v_p = \left[{\rm Re}\left(\frac{1}{v}\right)\right]^{-1}, \tag{A.2}$$

where v represents either $v_{\rm qP}$, $v_{\rm qSV}$ or $v_{\rm SH}$. The energy velocity vector of the qP and qSV waves is given by

$$\frac{\mathbf{v}_e}{v_p} = (l_1 + l_3\cot\psi)^{-1}\widehat{\mathbf{e}}_1 + (l_1\tan\psi + l_3)^{-1}\widehat{\mathbf{e}}_3 \tag{A.3}$$

(Carcione, 2007; Eq. (6.158)), where

$$\tan\psi = \frac{{\rm Re}(\beta^* X + \xi^* W)}{{\rm Re}(\beta^* W + \xi^* Z)} \tag{A.4}$$

defines the angle between the energy velocity vector and the z-axis, and

$$\beta = {\rm pv}\sqrt{A \pm B},$$

$$\xi = \pm\,{\rm pv}\sqrt{A \mp B},$$

$$B = \overline{p}_{11}l_1^2 - \overline{p}_{33}l_3^2 + \overline{p}_{55}\cos 2\theta, \tag{A.5}$$

where the upper and lower signs correspond to the qP and qSV waves, respectively. Moreover,

$$W = \overline{p}_{55}(\xi l_1 + \beta l_3),$$

$$X = \beta\overline{p}_{11}l_1 + \xi\overline{p}_{13}l_3,$$

$$Z = \beta\overline{p}_{13}l_1 + \xi\overline{p}_{33}l_3 \tag{A.6}$$

(Carcione, 2007; Eqs. (6.121)–(6.123)), where "pv" denotes the principal value, which has to be chosen according to established criteria (e.g., Sidler et al., 2008).

On the other hand, the energy velocity of the SH wave is

$$\mathbf{v}_e = \frac{v_p}{\rho{\rm Re}(v)}\left[l_1{\rm Re}\left(\frac{\overline{p}_{66}}{v}\right)\widehat{\mathbf{e}}_1 + l_3{\rm Re}\left(\frac{\overline{p}_{55}}{v}\right)\widehat{\mathbf{e}}_3\right] \tag{A.7}$$

and

$$\tan\psi = \frac{{\rm Re}(\overline{p}_{66}/v)}{{\rm Re}(\overline{p}_{55}/v)}\tan\theta \tag{A.8}$$

(Carcione, 2007; Eq. (4.115)). In general, the phase velocity is related to the energy velocity by

$$v_p = v_e \cos(\psi-\theta), \tag{A.9}$$

where $v_e = |\mathbf{v}_e|$. The quality factor is given by

$$Q = \frac{\mathrm{Re}(v^2)}{\mathrm{Im}(v^2)}. \tag{A.10}$$

The values of the qP quality factor along the layering plane and symmetry axis are

$$Q_P(\theta=\pi/2) = \frac{\mathrm{Re}(\overline{p}_{11})}{\mathrm{Im}(\overline{p}_{11})} \quad \text{and} \quad Q_P(\theta=0) = \frac{\mathrm{Re}(\overline{p}_{33})}{\mathrm{Im}(\overline{p}_{33})}, \tag{A.11}$$

respectively, while those of the shear waves are

$$Q_{SV}(\theta=\pi/2) = Q_{SV}(\theta=0) = Q_{SH}(\theta=0) = \frac{\mathrm{Re}(\overline{p}_{55})}{\mathrm{Im}(\overline{p}_{55})} \tag{A.12}$$

and

$$Q_{SH}(\theta=\pi/2) = \frac{\mathrm{Re}(\overline{p}_{66})}{\mathrm{Im}(\overline{p}_{66})}. \tag{A.13}$$

Appendix B. The stress–strain relation

Let σ_{ij} and $e_{ij}(u)$ denote the time Fourier transform of the stress and strain tensors of the viscoelastic material, where u is the displacement vector. For a medium composed of a sequence of TIV layers, $\Omega^{(n)}, n=1,\ldots,N$, the frequency-domain stress–strain relations on each Ω_n are (Carcione, 1992, 2007)

$$\sigma_{11}(u) = p_{11}^{(n)} e_{11}(u) + p_{12}^{(n)} e_{22}(u) + p_{13}^{(n)} e_{33}(u), \tag{B.1}$$

$$\sigma_{22}(u) = p_{12}^{(n)} e_{11}(u) + p_{11}^{(n)} e_{22}(u) + p_{13}^{(n)} e_{33}(u), \tag{B.2}$$

$$\sigma_{33}(u) = p_{13}^{(n)} e_{11}(u) + p_{13}^{(n)} e_{22}(u) + p_{33}^{(n)} e_{33}(u), \tag{B.3}$$

$$\sigma_{23}(u) = 2p_{55}^{(n)} e_{23}(u), \tag{B.4}$$

$$\sigma_{13}(u) = 2p_{55}^{(n)} e_{13}(u), \tag{B.5}$$

$$\sigma_{12}(u) = 2p_{66}^{(n)} e_{12}(u), \tag{B.6}$$

where $p_{ij}^{(n)}(\omega)$ are the complex coefficients for the n-layer.

The conversion between the Voigt stiffnesses and the stiffnesses of the 4th-rank tensors is

$$p_{IJ} = p_{ijkl},$$

$$I = i\delta_{ij} + (1-\delta_{ij})(9-i-j),$$

$$J = k\delta_{kl} + (1-\delta_{kl})(9-k-l), \tag{B.7}$$

where δ_{ij} denotes the Kronecker delta. The equation of motion is

$$\omega^2 \rho u(x,\omega) + \nabla \cdot \sigma(u(x,\omega)) = 0, \tag{B.8}$$

where σ is given by (B.1)–(B.6).

Let us consider x_1 and x_3 as the horizontal and vertical coordinates, respectively. As shown in Schoenberg and Muir (1989) the medium behaves as a homogeneous TIV medium at long wavelengths. Denoting by τ_{ij} the stress tensor of the equivalent TIV medium, the corresponding stress–strain relations, stated in the space–frequency domain, are (Carcione, 1992, 2007)

$$\tau_{11}(u) = \overline{p}_{11}\epsilon_{11}(u) + \overline{p}_{12}\epsilon_{22}(u) + \overline{p}_{13}\epsilon_{33}(u), \tag{B.9}$$

$$\tau_{22}(u) = \overline{p}_{12}\epsilon_{11}(u) + \overline{p}_{11}\epsilon_{22}(u) + \overline{p}_{13}\epsilon_{33}(u), \tag{B.10}$$

$$\tau_{33}(u) = \overline{p}_{13}\epsilon_{11}(u) + \overline{p}_{13}\epsilon_{22}(u) + \overline{p}_{33}\epsilon_{33}(u), \tag{B.11}$$

$$\tau_{23}(u) = 2\overline{p}_{55}\epsilon_{23}(u), \tag{B.12}$$

$$\tau_{13}(u) = 2\overline{p}_{55}\epsilon_{13}(u), \tag{B.13}$$

$$\tau_{12}(u) = 2\overline{p}_{66}\epsilon_{12}(u), \tag{B.14}$$

where ϵ_{ij} is the effective strain tensor and $\overline{p}_{IJ}$ are the complex and frequency-dependent Voigt stiffnesses given by Eq. (2.8), to be determined with the harmonic experiments.

References

Amirkhizi, A.V., Tehranian, A., Nemat-Nasser, S., 2010. Stress-wave energy management through material anisotropy. Wave Motion 47, 519–536.

Auld, B.A., 1990. Acoustic Fields and Waves in Solids, vol. 1. Krieger Publishing Company.

Backus, G.E., 1962. Long-wave elastic anisotropy produced by horizontal layering. Journal of Geophysical Research 67, 4427–4440.

Bayuk, I.O., Ammerman, M., Chesnokov, E.M., 2007. Elastic moduli of anisotropic clay. Geophysics 72, D107–D117.

Ben-Menahem, A.B., Singh, S.J., 1981. Seismic Waves and Sources. Springer-Verlag.

Bruggeman, D.A.G., 1937. Berechnung verschiedener physikalischer Konstanten von heterogenen Substanzen. III: Die elastischen Konstanten der quasi-isotropen Mischkörper aus isotropen Substanzen. Annalen der Physik 29, 160–178.

Carcione, J.M., 1992. Anisotropic Q and velocity dispersion of finely layered media. Geophysical Prospecting 40, 761–783.

Carcione, J.M., 2007. Wave fields in real media: wave propagation in anisotropic, anelastic, porous and electromagnetic media. Handbook of Geophysical Exploration, vol. 38, 2nd edition, revised and extended. Elsevier.

Carcione, J.M., 1990. Wave propagation in anisotropic linear viscoelastic media: theory and simulated wave fields. Geophysical Journal International 101, 739–750. (Erratum: 1992, 111, 191).

Carcione, J.M., Cavallini, F., 1994. A rheological model for anelastic anisotropic media with applications to seismic wave propagation. Geophysical Journal International 119, 338–348.

Carcione, J.M., Cavallini, F., 1995. Attenuation and quality factor surfaces in anisotropic-viscoelastic media. Mechanics of Materials 19, 311–327.

Carcione, J.M., Cavallini, F., Helbig, K., 1998. Anisotropic attenuation and material symmetry. Acustica 84, 495–502.

Carcione, J.M., Kosloff, D., Behle, A., 1991. Long-wave anisotropy in stratified media: a numerical test. Geophysics 56, 245–254.

Carcione, J.M., Santos, J.E., Picotti, S., 2011. Anisotropic poroelasticity and wave-induced fluid flow. Harmonic finite-element simulations. Geophysical Journal International 186 (3), 1245–1254.

Carlson, R.L., Christensen, N.I., 1979. Velocity anisotropy in semi-indurated calcareous deep sea sediments. Journal of Geophysical Research 84, 205–211.

Carlson, R.L., Schaftenaar, C.H., Moore, R.P., 1984. Causes of compressional-wave anisotropy in carbonate-bearing deep sea sediment. Geophysics 49, 525–532.

Hudson, J.A., Crampin, S., 1991. On: "A calculus for finely layered anisotropic media" by M. Schoenberg and F. Muir (Geophysics, 54, 581–589, May 1989), Geophysics 56, 575, doi: 10.1190/1.1486691.

Kolsky, H., 1963. Stress Waves in Solids. Dover publications, New York.

Krzikalla, F., Müller, T., 2010. Anisotropic P–SV-wave dispersion and attenuation due to inter-layer flow in thinly layered porous rocks. Geophysics 76 (3), WA135–WA145.

Liu, H.P., Anderson, D.L., Kanamori, H., 1976. Velocity dispersion due to anelasticity; implications for seismology and mantle composition. Geophysical Journal of the Royal Astronomical Society 47, 41–58.

Picotti, S., Carcione, J.M., Santos, J.E., Gei, D., 2010. Q-anisotropy in finely-layered media. Geophysical Research Letters 37, L06302. doi:10.1029/2009GL042046.

Postma, G.W., 1955. Wave propagation in a stratified medium. Geophysics 20, 780–806.

Revil, A., Grauls, D., Brévart, O., 2002. Mechanical compaction of sand/clay mixtures. Journal of Geophysical Research 107, 2293–2308. doi:10.1029/2001JB000318.

Riznichenko, Y.V., 1949. Seismic quasi-anisotropy. Bulletin of the Russian Academy of Sciences, Geographical and Geophysical Service 13, 518–544.

Santos, J.E., Carcione, J.M., Picotti, S., 2011. Viscoelastic-stiffness tensor of anisotropic media from oscillatory numerical experiments. Computer Methods in Applied Mechanics and Engineering 200, 896–904.

Schoenberg, M., Muir, F., 1989. A calculus for finely layered media. Geophysics 54, 581–589.

Sidler, R., Carcione, J.M., Holliger, K., 2008. On the evaluation of the plane-wave reflection coefficients in anelastic media. Geophysical Journal International 175, 94–102.

Thomsen, L., 1986. Weak elastic anisotropy. Geophysics 51, 1954–1966.

Wang, Z., 2002. Seismic anisotropy in sedimentary rocks. Part 2: laboratory data. Geophysics 67, 1423–1440.